# Instabilities in the oscillatory flow of a complex fluid

M. Torralba,[1] A. A. Castrejón-Pita,[2,*] G. Hernández,[2] G. Huelsz,[2] J. A. del Río,[2] and J. Ortín[1]
[1]*Departament ECM, Facultat de Física, Universitat de Barcelona, Avenida Diagonal 647, E-08028 Barcelona, Catalonia, Spain*
[2]*Centro de Investigación en Energía, Universidad Nacional Autónoma de México, Apartado Postal 34, 62580 Temixco (Morelos), Mexico*
(Received 10 January 2007; published 17 May 2007)

The dynamics of a fluid in a vertical tube, subjected to an oscillatory pressure gradient, is studied experimentally for both a Newtonian and a viscoelastic shear-thinning fluid. Particle image velocimetry is used to determine the two-dimensional velocity fields in the vertical plane of the tube axis, in a range of driving amplitudes from 0.8 to 2.5 mm and of driving frequencies from 2.0 to 11.5 Hz. The Newtonian fluid exhibits a laminar flow regime, independent of the axial position, in the whole range of drivings. For the complex fluid, instead, the parallel shear flow regime exhibited at low amplitudes [Torralba *et al.*, Phys. Rev. E **72**, 016308 (2005)] becomes unstable at higher drivings against the formation of symmetric vortices, equally spaced along the tube. At even higher drivings the vortex structure itself becomes unstable, and complex nonsymmetric structures develop. Given that inertial effects remain negligible even at the hardest drivings ($\mathrm{Re} < 10^{-1}$), it is the complex rheology of the fluid that is responsible for the instabilities observed. The system studied represents an interesting example of the development of shear-induced instabilities in nonlinear complex fluids in purely parallel shear flow.

DOI: 10.1103/PhysRevE.75.056307 PACS number(s): 47.50.−d, 47.60.+i, 83.60.Wc

## I. INTRODUCTION

The oscillatory flow of a viscoelastic (complex) fluid is remarkably different from that of a Newtonian (simple) fluid, even at very low driving amplitudes. In particular, it has been predicted theoretically [1,2] and demonstrated experimentally [3] that the response of a viscoelastic fluid in a vertical tube to an oscillatory pressure gradient—measured by the flow velocity at the tube axis, for a given amplitude of the pressure gradient—exhibits very large resonance peaks at particular driving frequencies. The resonant behavior of the viscoelastic-fluid–tube system is in striking contrast with the purely dissipative response of a Newtonian fluid in the same experimental conditions.

The structure of the oscillatory flow in the tube is also much more complex for the viscoelastic fluid than for the Newtonian one, even at very low driving amplitudes [4]. At sufficiently low driving amplitudes [Reynolds number (Re) $< 10^{-3}$] a purely parallel shear flow, with the axial symmetry of the tube and the periodicity of the driving, is established in both cases. However, while for the Newtonian fluid the instantaneous velocity field has the same sign everywhere, for the viscoelastic fluid the flow resolves into annular regions of alternating upward and downward motion. These regions are separated by quiescent boundaries (nodes of the velocity profile in the radial direction of the tube), where shear stresses reach local maxima. The quiescent cylindrical boundaries remain static, and their number increases with increasing driving frequency, in such a way that an additional annular region of flow is present at each new resonance frequency [4]. All these features are well captured by a linear theory based on a linear approximation of the hydrodynamic equations, where inertial effects are neglected, and a linear Maxwell model is used as constitutive equation of the viscoelastic fluid [1,3].

The study of an oscillatory flow in a circular cross section finds applications in several branches of technology. Oscillatory flows have been proposed for stimulation of oil reservoirs [5], for reducing wetting layers of viscoelastic fluids [6], and also for the treatment of groundwater aquifers contaminated by organic liquids, using elastic waves [7]. Oscillatory flows are also present in the circulatory and breathing system of living creatures [8], where it has been suggested that the pumping frequency is selected to provide maximum power [7].

The aim of the present investigation is to explore experimentally in which ways the basic parallel shear flow described above becomes unstable as the fluid is subjected to a harder oscillatory driving, by increasing the forcing amplitude and/or the forcing frequency. We focus on driving frequencies that correspond to either maxima or minima of the viscoelastic fluid response. In all instances the Reynolds number remains very small ($\mathrm{Re} < 10^{-1}$), ensuring that the increasing complexity of the flow (in the case of the viscoelastic fluid) is due to the rheological properties of the fluid, not to inertial effects. This is a natural extension of our previous work in this field [3,4]. In all cases we analyze the flow sufficiently far from the two ends of the system (the piston and the free surface). Another important motivation comes from the fact that, although parallel shear flows of viscoelastic fluids are acknowledged to be linearly stable [9], Morozov and van Saarloos have demonstrated very recently that plane Couette flow undergoes a purely elastic subcritical instability, by which a small finite-size perturbation is sufficient to create a secondary flow [10]. Our system exhibits a parallel shear flow, with shear stresses accumulating near the quiescent cylindrical boundaries, and as such it is a promising candidate to exhibit a similar kind of nonlinear elastic instability.

*Present address: Atmospheric, Oceanic and Planetary Physics, Clarendon Laboratory, University of Oxford, Parks Road, Oxford, OX1 3PU, U.K.

 

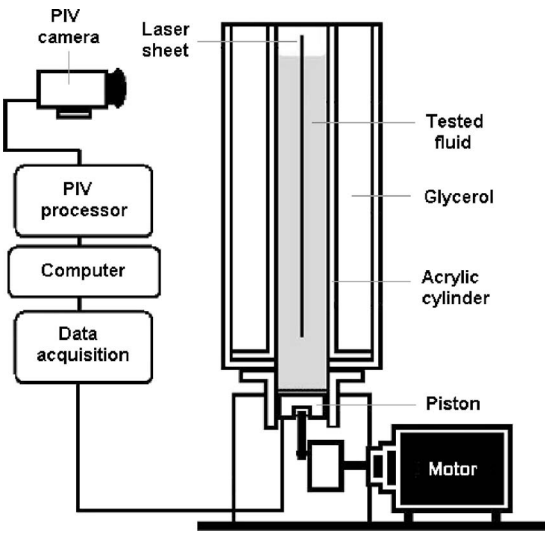


FIG. 1. Schematic view of the experimental device, including the setup for particle image velocimetry (PIV) measurements.

## II. EXPERIMENT

In this section we review briefly our experimental setup, the properties of the fluids considered, and the measurement techniques used.

The experimental device (Fig. 1) consists of a vertical cylinder made of transparent acrylic, of inner radius $a=25$ mm and height 500 mm, filled with the test fluid. In order to avoid optical aberrations, this cylinder is placed inside a second recipient of transparent acrylic, of square section, filled with glycerol to match the refractive index of the acrylic walls. A Teflon piston at the bottom end of the cylinder, driven by a motor of variable frequency, produces harmonic oscillations of the pressure gradient in the liquid column. The amplitude of the oscillation can be modified by changing the eccentricity of the driving wheel. Amplitudes of 0.8, 1.2, 1.6, 2.0, and 2.5 (±0.05) mm have been studied.

We have chosen a silicone oil of nominal dynamic viscosity $\eta=56$ Pa s and density $\rho=973$ kg/m$^3$, at the working temperature of 25±0.5 °C, as Newtonian fluid. The viscoelastic fluid is an aqueous solution of cetylpyridinium chloride (CPyCl) 100 mM and sodium salicylate (NaSal) 60 mM. In a range of concentrations, including the 100-60 considered here, this surfactant solution forms wormlike micelles and exhibits the rheological behavior of a linear Maxwell fluid [11,12]. In our case the solution has dynamic viscosity $\eta=60$ Pa s, density $\rho=1050$ kg/m$^3$, and Maxwell relaxation time $t_m=1.9$ s, at the working temperature of 25±0.5 °C. At high shear rates ($\dot{\gamma}>0.1$ s$^{-1}$) the fluid exhibits shear thinning [13].

The velocity fields in a vertical plane, along the symmetry axis of the tube, have been measured by two-dimensional (2D) particle image velocimetry (PIV) [14]. The fluid is seeded with Dantec 20 $\mu$m polyamide spheres. Dual-pulsed neodymium-doped yttrium aluminum garnet (Nd:YAG) lasers are used to illuminate the interrogation plane, of about 1 mm thickness. Two consecutive frames, one corresponding to each laser light pulse, are recorded with a digital camera (spatial resolution $1008\times1016$ pixels), at an acquisition rate of 15 pairs of images per second (15 Hz). The velocity maps are obtained by data postprocessing, measuring the statistical displacement of the seeding particles in the fluid in the time interval between two consecutive laser pulses, using the Dantec FLOW MAP software.

Our measurements have been performed in an interrogation plane of $50\times50$ mm$^2$, at about 250 mm (five tube diameters) from the neutral position of the piston. This distance is large enough to ensure that the flow in the interrogation plane does not feel the proximity of the piston. By covering the fluid surface at the top end of the tube with a cover lid, we have verified that oscillations of the free surface do not have any measurable effect on the flow in the region of interest.

The 2D PIV technique provides only the two in-plane components of the actual 3D velocity field in the interrogation plane, in a vertical section of the tube. This information is complete only if the velocity field is contained within the interrogation plane and the flow is axisymmetric. We investigate whether this is the case in our experiments by checking whether the velocity field in the interrogation plane satisfies $\vec{\nabla}\cdot\vec{v}=0$ (within experimental error), meaning that the velocity component perpendicular to the interrogation plane is negligible. The background (zero) level of $\vec{\nabla}\cdot\vec{v}$ is determined by the laminar base flow, for which the radial and azimuthal components of $\vec{v}$ are 0 and the vertical component of $\vec{v}$ depends only on the radius.

TABLE I. Summary of PIV results for the 100:60 CPyCl-NaSal solution. $z_0$ and $\nu$ are driving amplitude and frequency. At each driving frequency, the behavior of the dynamic response of the viscoelastic-fluid–tube system and the number of internal nodes observed in the laminar regime (away from the tube wall) are also indicated. Vortex-s and vortex-ns indicate symmetric and nonsymmetric vortices, respectively.

| Dynamic response | Internal nodes | $z_0$ (mm) / $\nu$ (Hz) | 0.8 | 1.2 | 1.6 | 2.0 | 2.5 |
|---|---|---|---|---|---|---|---|
| | | | Flow structure | | | | |
| Maximum | 0 | 2.0 | Laminar | Laminar | Laminar | Laminar | Laminar |
| Minimum | 0 | 3.5 | Laminar | Laminar | Laminar | Laminar | Laminar |
| Maximum | 2 | 6.5 | Laminar | Fluctuating laminar | Vortex-s | Vortex-s | Vortex-ns |
| Minimum | 2 | 8.2 | Laminar | Vortex-s | Vortex-s | Vortex-ns | Vortex-ns |
| Maximum | 4 | 10.5 | Laminar | Fluctuating laminar | Vortex-s | Vortex-ns | Vortex-ns |
| Minimum | 4 | 11.5 | Laminar | Vortex-s | Vortex-s | Vortex-ns | Vortex-ns |

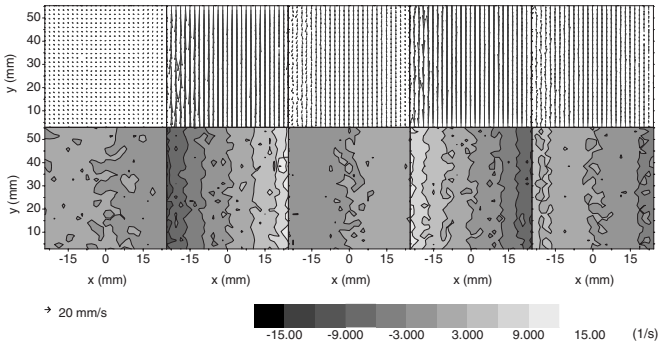


FIG. 2. Silicone oil: PIV results for $\nu=8.2$ Hz and $z_0=1.2$ mm ($\mathrm{Re}=3\times10^{-2}$). Top: velocity vector field. Bottom: azimuthal vorticity contours. The corresponding scales are given by the little arrow and the gray level scale at the bottom of the figure.

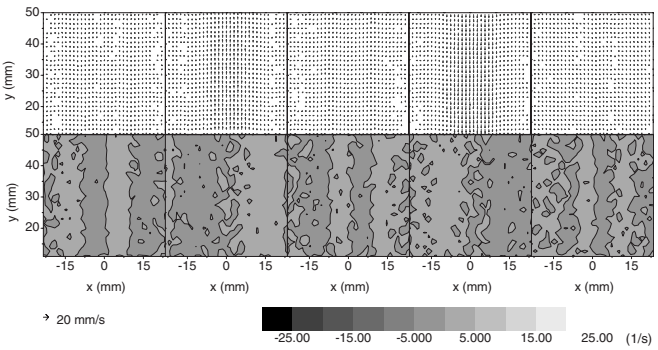


FIG. 3. 100:60 CPyCl-NaSal solution: PIV results for $\nu=2.0$ Hz and $z_0=0.8$ mm ($\mathrm{Re}=4\times10^{-3}$, $\mathrm{Wi}=0.8$). Top: velocity vector field. Bottom: azimuthal vorticity contours. The corresponding scales are given by the little arrow and the gray level scale at the bottom of the figure.

Wormlike micellar solutions are known to be birefringent. A number of authors have used this property to visualize the stress field in flows of these non-Newtonian fluids [15,16]. In our case, since the light sheet of the interrogation plane is already polarized, it suffices to place a polarizer on the front wall of the acrylic box containing the tube. The state of repose is chosen as reference state to set the orientation of the polarizer. Birefringence measurements have been acquired at a sampling rate of one image every 2.667 s. Qualitative representations of the stress field in the flow have been obtained in this way, and compared to their velocity field counterparts.

## III. RESULTS

The oscillating flow in the tube has been studied at driving frequencies that coincide with either the first three maxima in the dynamic response of the complex-fluid–tube system (first three resonance frequencies), 2.0, 6.5, and 10.5(±0.1)Hz, or the first three minima, 3.5, 8.2, and 11.5(±0.1)Hz [4].

The PIV measurements of the Newtonian fluid show that the flow remains laminar in the whole range of driving parameters explored in the present investigation. The results are presented in Sec. III A 1. This is not the case for the viscoelastic fluid. Table I provides a summary of the flow structures observed at different values of the driving parameters. Laminar flows are described in Sec. III A 2, and more complex flows in Sec. III B.

The PIV acquisition rate is very low compared to the driving frequency. Actually, we cannot acquire a significant number of image pairs in a single oscillation period for any of the driving frequencies. In practice, we acquire pairs of images at the maximum affordable rate. We fold PIV measurements back to the first period during data postprocessing. This strategy optimizes the temporal resolution of our experiments within a driving period, assuming that the flow follows exactly the periodicity of the driving (see the discussion in Sec. III C 1) and it has been adopted in all the measurements presented below.

The relevant dimensionless numbers that characterize the flow at given driving amplitude and frequency are the following.

*Reynolds number*. The Reynolds number measures the ratio of inertial to viscous forces. In our system Re can be defined as $\mathrm{Re}=\rho 2\pi\nu z_0 a/\eta$, where $\nu$ and $z_0$ are the driving frequency and amplitude. For the values of $\nu$ and $z_0$ explored in the present experiments Re is very small, in the range $4\times10^{-3}$ to $8\times10^{-2}$, ensuring that inertia is not responsible for the destabilization of the basic flow. If the decrease in $\eta$ due to shear thinning is taken into account, Re increases by about two orders of magnitude, but remains much smaller than the critical value for which the oscillatory flow of a Newtonian fluid would become unstable [17].

*Stokes parameter*. For an oscillatory viscous flow in a tube, the Stokes parameter ($\Lambda$) measures the ratio of the tube radius to the viscous penetration depth $\Lambda=a/\delta_\nu$, where $\delta_\nu=\sqrt{\eta/(\rho\pi\nu)}$ [17]. For all the experiments reported here $\Lambda<2$, which means that all the flow is influenced by the tube wall, i.e., viscous oscillatory boundary layers occupy all the tube.

*Deborah number*. For a viscoelastic fluid, the relative importance of the relaxation time of the fluid to the time scale of the flow is measured by the Deborah number $\mathrm{De}=t_m\eta/(a^2\rho)$. In our case $\mathrm{De}=174\gg1$, so that elasticity of the viscoelastic fluid is important enough for resonances to occur. The decrease in $\eta$ due to shear thinning still leads to a minimum $\mathrm{De}\gg1$. It is also worth noting that, if the frequencies are made dimensionless in the form $2\pi\nu\tau$, where the characteristic time $\tau=10^{2/5}t_m\sqrt{1/\mathrm{De}}$, the dimensionless resonance frequencies become universal, i.e., independent of fluid parameters and system dimensions [1].

*Weissenberg number*. The Weissenberg (Wi) number is the ratio of the relaxation time of the fluid to a characteristic inverse shear rate, $\mathrm{Wi}=t_m\dot{\gamma}$, where the shear rate gives the relative velocity of two fluid layers moving with respect to each other. A value $\mathrm{Wi}\gtrsim1$ indicates that elastic stresses become large. Thus, the onset of elastic instability of a basic laminar flow is characterized by a critical Wi [9,18]. We define the characteristic shear rate as the ratio between the velocity of the piston and the distance $r_q$ between the tube axis and the first quiescent point of the flow [4]:

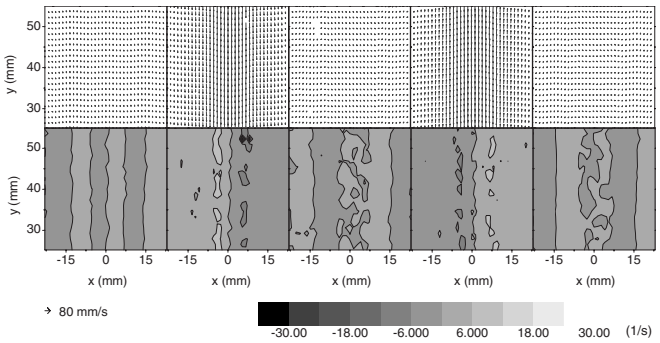


FIG. 4. 100:60 CPyCl-NaSal solution: PIV results for $\nu$ =2.0 Hz and $z_0$=2.5 mm (Re=$10^{-2}$, Wi=2.4). Top: velocity vector field. Bottom: azimuthal vorticity contours. The corresponding scales are given by the little arrow and the gray level scale at the bottom of the figure.

$$\dot{\gamma}_{char} \equiv \frac{2\pi\nu z_0}{r_q}. \tag{1}$$

For the experiments reported here, Wi takes values between 0.7 and 60.

### A. Basic flow

Our PIV measurements of the basic (laminar) flow, for both silicone oil and the 100:60 CPyCl-NaSal aqueous solution, are presented here. The behavior for a driving amplitude $z_0$=0.8 mm and $\nu$=2.0,6.5,10.0 Hz has already been described in detail in Ref. [4] and reviewed in the Introduction. We focus therefore on new results for other frequencies at the same amplitude, and for higher amplitudes. It is important to notice that the viscosity of the silicone oil is very similar to the viscosity of the surfactant solution, so that the main difference between both fluids is the elasticity of the surfactant solution. The following figures represent the flow at time phases 0, $T/4$, $T/2$, $3T/4$, and $T$.

#### *1. Newtonian fluid: Silicone oil*

For the Newtonian fluid, silicone oil, the flow remains laminar at all the amplitudes and frequencies explored in the present investigation.

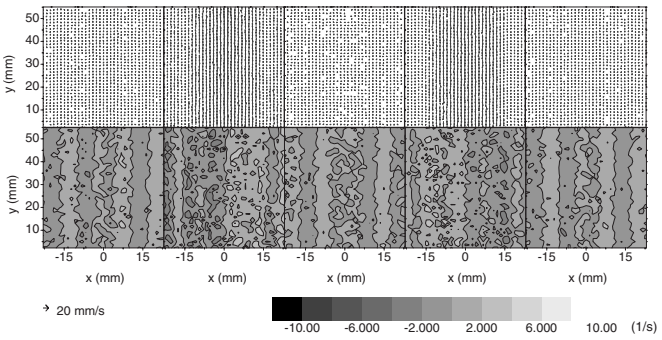


FIG. 5. 100:60 CPyCl-NaSal solution: PIV results for $\nu$ =3.5 Hz and $z_0$=0.8 mm (Re=$8\times10^{-3}$, Wi=1.3). Top: velocity vector field. Bottom: azimuthal vorticity contours. The corresponding scales are given by the little arrow and the gray level scale at the bottom of the figure.

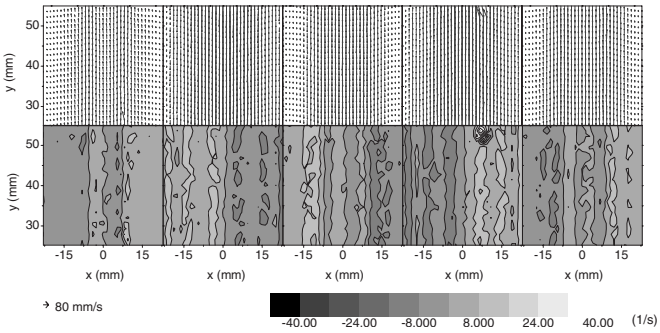


FIG. 6. 100:60 CPyCl-NaSal solution: PIV results for $\nu$ =3.5 Hz and $z_0$=2.5 mm (Re=$2\times10^{-2}$, Wi=4.2). Top: velocity vector field. Bottom: azimuthal vorticity contours. The corresponding scales are given by the little arrow and the gray level scale at the bottom of the figure.

Figure 2 presents the velocity vector field for a driving amplitude of 1.2 mm and a driving frequency of 8.2 Hz. The results show that a parallel shear flow is established. The fluid oscillates in the tube following the periodicity of the driving. All fluid elements in the interrogation plane move instantaneously in the same direction, the velocity approaching zero near the tube boundaries.

Our experimental results show that this laminar flow is always stable for all the frequencies explored and up to a driving amplitude of 10 mm.

#### *2. Viscoelastic fluid: 100:60 CPyCl-NaSal aqueous solution*

As discussed in the Introduction, the basic (laminar) flow of the viscoelastic fluid consists of annular regions of alternating upward and downward motion, separated by quiescent boundaries [4]. Shear stresses concentrate at these quiescent boundaries and increase as the magnitude of the driving increases.

According to Table I, the viscoelastic flow remains laminar at all amplitudes for the two lower driving frequencies explored, 2.0 and 3.5 Hz. Figures 3–6 show our results for the two extreme driving amplitudes 0.8 and 2.5 mm. This observation is related to the fact that the number of annular

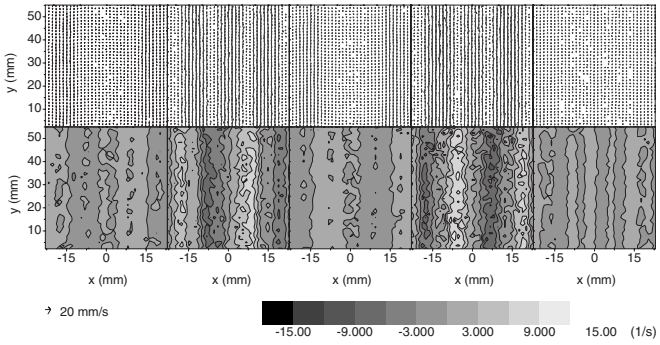


FIG. 7. 100:60 CPyCl-NaSal solution: PIV results for $\nu$ =8.2 Hz and $z_0$=0.8 mm (Re=$2\times10^{-2}$, Wi=12.8). Top: velocity vector field. Bottom: azimuthal vorticity contours. The corresponding scales are given by the little arrow and the gray level scale at the bottom of the figure.

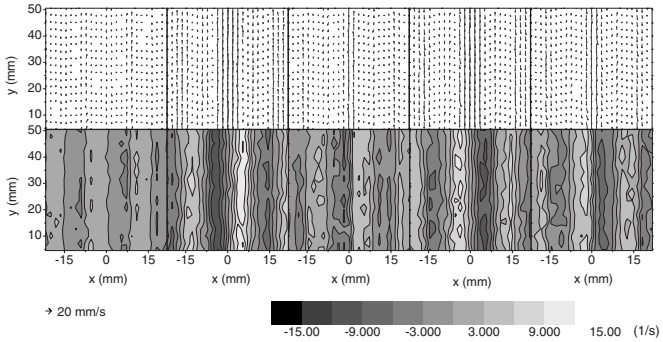


FIG. 8. 100:60 CPyCl-NaSal solution: PIV results for $\nu=11.5$ Hz and $z_0=0.8$ mm ($\mathrm{Re}=3\times10^{-2}$, $\mathrm{Wi}=18.6$). Top: velocity vector field. Bottom: azimuthal vorticity contours. The corresponding scales are given by the little arrow and the gray level scale at the bottom of the figure.

regions does not depend on driving amplitude, as predicted by a linear theory valid at low driving amplitudes [4].

The number of alternating annular regions increases with driving frequency. At a driving amplitude of 0.8 mm, however, the flow remains laminar at all frequencies. Results for the resonance frequencies 6.5 and 10.5 Hz were already presented in Ref. [4]. Results for the frequencies 8.2 and 11.5 Hz (minima of the dynamic response) are shown in Figs. 7 and 8.

The azimuthal vorticity contours reveal that the vorticity, as expected, concentrates at the vertical lines where the flow is quiescent. These are cuts of the actual cylindrical vortex sheets associated with the quiescent cylindrical boundaries.

### B. Flow instabilities

Table I shows that the viscoelastic flow becomes unstable at $\nu=6.5$ Hz (second resonance frequency), $z_0=1.2$ mm, and at all higher frequencies and amplitudes.

At the onset of instability ($\nu=6.5$ Hz, $z_0=1.2$ mm) the laminar flow exhibits modulations of the vertical streamlines, already visible in Fig. 9. At $\nu=10.5$ Hz, $z_0=1.2$ mm, i.e., at the next resonance frequency and same amplitude, another

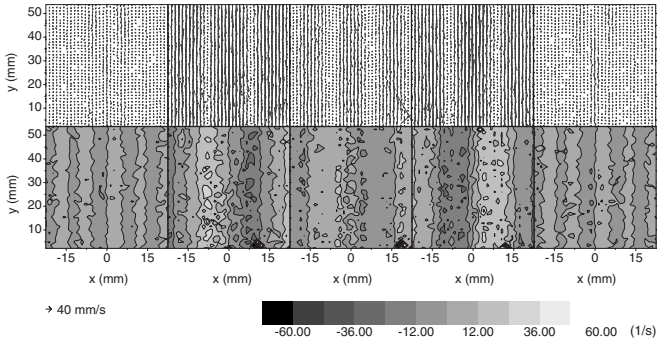


FIG. 9. 100:60 CPyCl-NaSal solution: PIV results for $\nu=6.5$ Hz and $z_0=1.2$ mm ($\mathrm{Re}=2\times10^{-2}$, $\mathrm{Wi}=11.4$). Top: velocity vector field. Bottom: azimuthal vorticity contours. The corresponding scales are given by the little arrow and the gray level scale at the bottom of the figure.

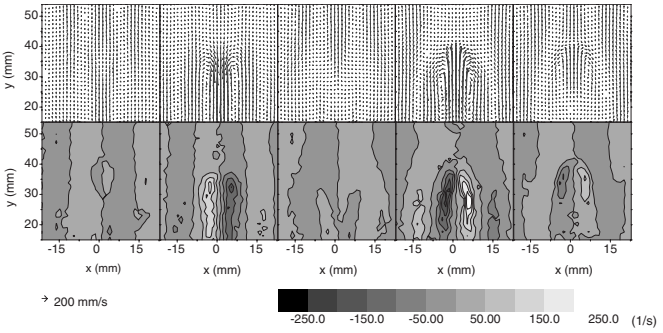


FIG. 10. 100:60 CPyCl-NaSal solution: PIV results for $\nu=8.2$ Hz and $z_0=1.2$ mm ($\mathrm{Re}=3\times10^{-2}$, $\mathrm{Wi}=19.3$). Top: velocity vector field. Bottom: azimuthal vorticity contours. The corresponding scales are given by the little arrow and the gray level scale at the bottom of the figure.

annular region has formed (two new nodes), and modulations of the vertical streamlines are also observed.

Interestingly, at the intermediate frequency $\nu=8.2$ Hz and at the same amplitude $z_0=1.2$ mm, the flow presents two stationary symmetric vortices (vortex-s) (Fig. 10). The two vortices are centered at the two nodes of the base flow closer to the tube axis, and change their rotation direction every half period of the driving.

By taking low-resolution PIV measurements in a larger image area, we have found that several equidistant toroidal vortices form along the tube, with a center-to-center separation of about 2.5 tube radius for a forcing frequency of 8.2 Hz, and of 1.25 tube radius for a forcing frequency of 11.5 Hz. Figure 11 shows an example.

The cylindrical symmetry of the flow is still preserved at the onset of instability. This has been verified by repeating the measurements several times from the state of repose. Therefore Fig. 10 is actually showing a transverse cut of a toroidal vortex around the symmetry axis of the tube. This is also true for the experiments at a driving amplitude of 1.6 mm (Figs. 12 and 13), and for the experiment at 6.5 Hz and 2.0 mm (Fig. 14).

For stationary symmetric vortices the radial coordinate of the vortex center is independent of driving amplitude (Fig.

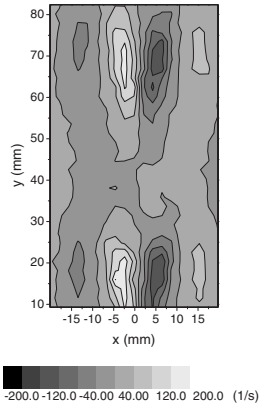


FIG. 11. Low-resolution azimuthal vorticity contours for the 100:60 CPyCl-NaSal solution driven at $\nu=8.2$ Hz and $z_0=1.2$ mm ($\mathrm{Re}=3\times10^{-2}$, $\mathrm{Wi}=19.3$), showing that several toroidal vortices form along the tube.

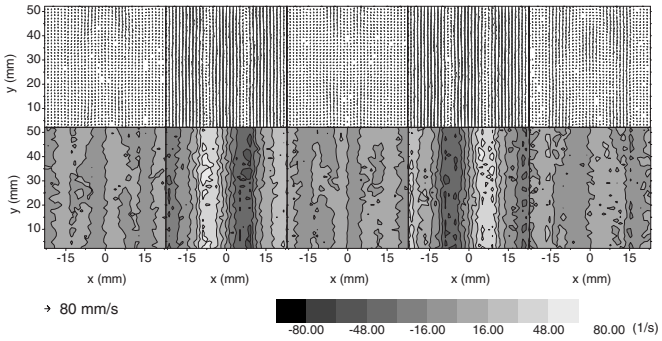


FIG. 12. 100:60 CPyCl-NaSal solution: PIV results for $\nu$ =6.5 Hz and $z_0$=1.6 mm (Re=$3\times10^{-2}$, Wi=15.1). Top: velocity vector field. Bottom: azimuthal vorticity contours. The corresponding scales are given by the little arrow and the gray level scale at the bottom of the figure.

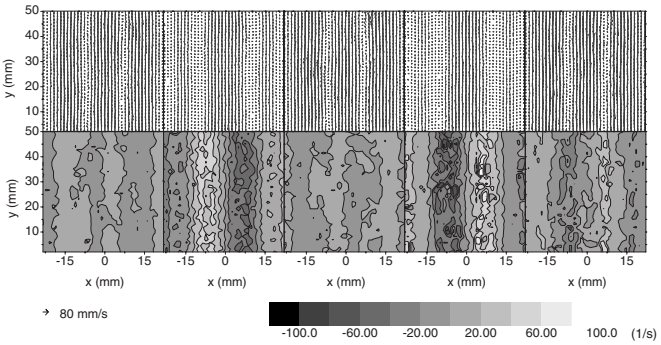


FIG. 14. 100:60 CPyCl-NaSal solution: PIV results for $\nu$ =6.5 Hz and $z_0$=2.0 mm (Re=$4\times10^{-2}$, Wi=18.9). Top: velocity vector field. Bottom: azimuthal vorticity contours. The corresponding scales are given by the little arrow and the gray level scale at the bottom of the figure.

15) but strongly dependent on driving frequency. As the driving frequency is increased the vortex center approaches the center of the tube, following the behavior of the quiescent flow points (Fig. 15). It is also interesting to notice that the presence of these symmetric vortices does not modify the location of the quiescent flow points.

As the driving increases further, the vortices get distorted and lead to more complex nonsymmetric structures (vortex-ns). At forcings of 2.0 mm, 8.2 (Fig. 16), 10.5, and 11.5 Hz, and at forcings of 2.5 mm, 8.2 Hz the vortices form very close to the tube axis and are heavily distorted, but their center does not move in time. At this same amplitude (2.5 mm) and at forcing frequencies of 6.5, 10.5, and 11.5 Hz, we observe nonsymmetric and nonstationary vortices. Figure 17 shows that the flow loses its axial symmetry and, furthermore, the non-negligible magnitude of the local divergence at the vortices reveals that the velocity field at the vortices presents an azimuthal component.

### C. Velocity fluctuations

An integrated (global) measure of the destabilization of the basic laminar flow is given by the rms fluctuations of the $r$ and $z$ components of the velocity along the vertical direction. For convenience, we use Cartesian coordinates $v_x$ and $v_y$. We define

$$\sigma_{v_x}(x,t) = \sqrt{\frac{1}{N}\sum_i [v_x(x,y_i,t) - \overline{v_x}(x,t)]^2}, \tag{2}$$

$$\sigma_{v_y}(x,t) = \sqrt{\frac{1}{N}\sum_i [v_y(x,y_i,t) - \overline{v_y}(x,t)]^2}, \tag{3}$$

where $\overline{v_x}(x,t)$ and $\overline{v_y}(x,t)$ are the velocity components averaged along the vertical ($y$) direction and $N$ is the number of velocity measurements in the image plane along the vertical direction. Although the magnitude of $\sigma_{v_y}$ is usually higher than $\sigma_{v_x}$, both magnitudes behave very similarly. Finally, to make the rms fluctuations comparable for different magnitudes of the forcing we make them dimensionless in the form

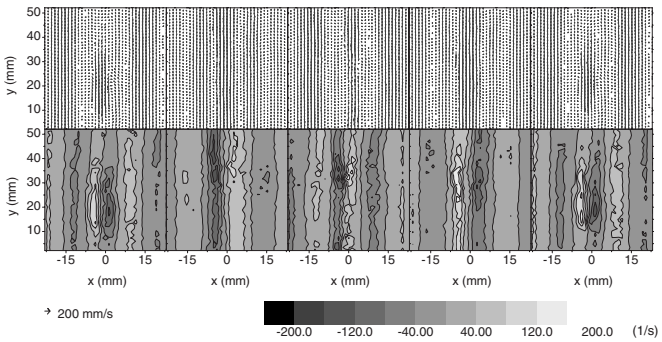


FIG. 13. 100:60 CPyCl-NaSal solution: PIV results for $\nu$ =8.2 Hz and $z_0$=1.6 mm (Re=$4\times10^{-2}$, Wi=25.7). Top: velocity vector field. Bottom: azimuthal vorticity contours. The corresponding scales are given by the little arrow and the gray level scale at the bottom of the figure.

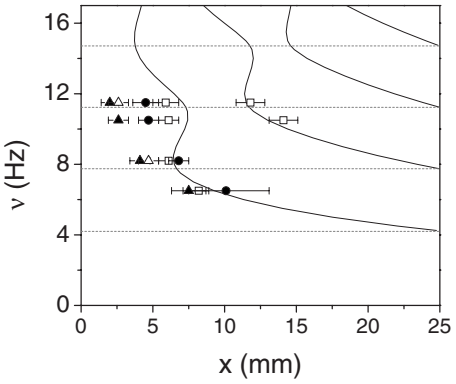


FIG. 15. Location of the quiescent flow points along the radial coordinate $x$ (solid lines), and minima of the permeability (dashed horizontal lines), as derived from a linear theory. The parameters $\rho$, $\eta$, and $t_m$ used to calculate the diagram are those given for CPyCl-NaSal 100:60 in the text, and the radius of the cylinder is $a$ =25 mm. The different symbols (experimental data) give the radial location of the quiescent points of the flow, for $z_0$=0.8 mm (□); the maxima of the vorticity closer to the center of the tube, for $z_0$ =0.8 mm (●); the vortex center, for $z_0$=1.2 mm (△) and $z_0$ =1.6 mm (▲).

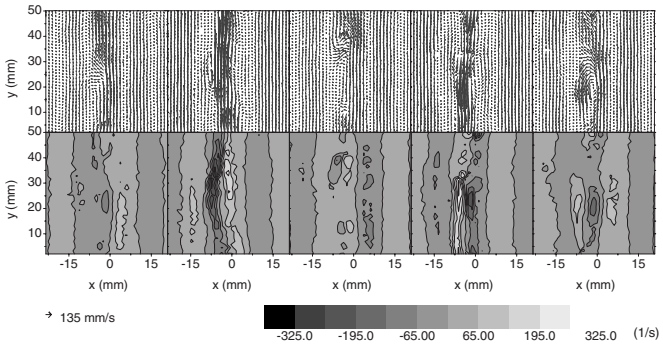


FIG. 16. 100:60 CPyCl-NaSal solution: PIV results for $\nu$ =8.2 Hz and $z_0$=2.0 mm (Re=$5\times10^{-2}$, Wi=32.1). Top: velocity vector field. Bottom: azimuthal vorticity contours. The corresponding scales are given by the little arrow and the gray level scale at the bottom of the figure.

$$\tilde{\sigma}_{v_x}(x,t) = \frac{\sigma_{v_x}(x,t)}{2\pi\nu z_0}, \tag{4}$$

$$\tilde{\sigma}_{v_y}(x,t) = \frac{\sigma_{v_y}(x,t)}{2\pi\nu z_0}. \tag{5}$$

#### 1. Space averages

The time dependence of the velocity fluctuations is computed by averaging $\tilde{\sigma}_{v_x}(x,t)$ and $\tilde{\sigma}_{v_y}(x,t)$ along the radial direction $x$.

If a velocity component follows the periodicity of the driving, its rms fluctuations are periodic as well, with a frequency two times the driving frequency. This is visible in Fig. 18, which shows the $x$-averaged rms fluctuations of the $y$ component of the velocity vs time, $\tilde{\sigma}_{v_y}(t)$, for the viscoelastic fluid driven at 8.2 Hz. The correlation between adjacent

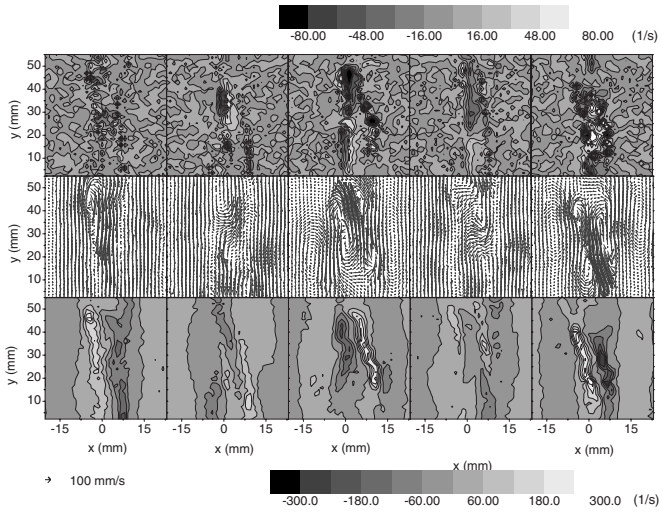


FIG. 17. 100:60 CPyCl-NaSal solution: PIV results for $\nu$ =6.5 Hz and $z_0$=2.5 mm (Re=$4\times10^{-2}$, Wi=40.1). Top: local divergence. Middle: velocity vector field. Bottom: azimuthal vorticity contours. The corresponding scales are given by the little arrow and the two gray level scales.

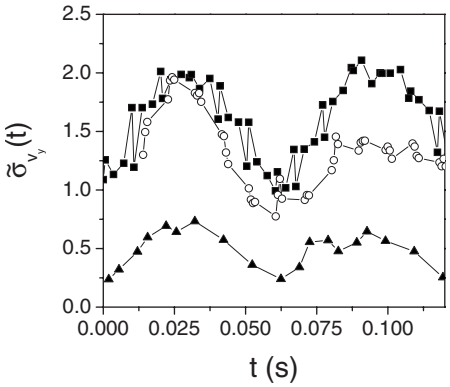


FIG. 18. 100:60 CPyCl-NaSal solution: $x$-averaged rms fluctuations of the $y$ component of the velocity as a function of time, $\tilde{\sigma}_{v_y}(t)$, for the viscoelastic fluid driven at 8.2 Hz and amplitudes $z_0$=0.8 (▲), $z_0$=1.6 (○), and 2.0 mm (■).

points validates the procedure of folding the PIV data back to the first oscillation period, thus confirming that even this nonlaminar flow follows the periodicity of the basic flow. We must say that for a forcing frequency of 10.5 Hz the correlation between adjacent points is worse than the correlation observed at other frequencies.

#### 2. Time averages

The spatial dependence of the velocity fluctuations is computed by averaging $\tilde{\sigma}_{v_x}(x,t)$ and $\tilde{\sigma}_{v_y}(x,t)$ in a time pe-

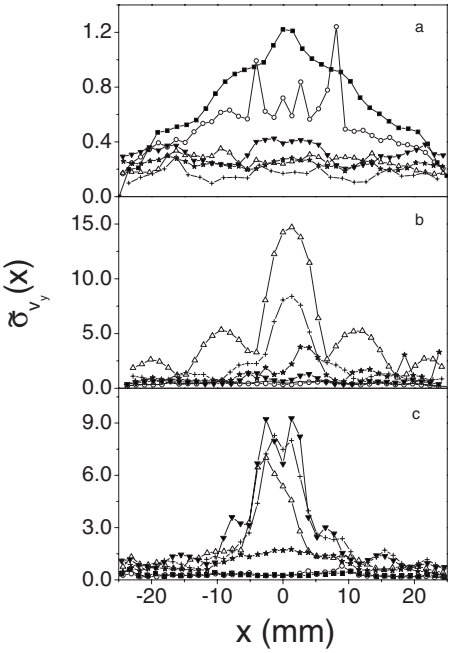


FIG. 19. 100:60 CPyCl-NaSal solution: time-averaged rms fluctuations of the $y$ component of the velocity, $\tilde{\sigma}_{v_y}(x)$, as a function of the radial coordinate $x$ for the viscoelastic fluid driven at an amplitude (a) 0.8, (b) 1.2, and (c) 1.6 mm. The symbols correspond to the different driving frequencies (in Hz) 2.0 (■), 3.5 (○), 6.5 (⋆), 8.2 (△), 10.5 (▼), and 11.5 (+). Notice the different magnitude of the vertical scales.

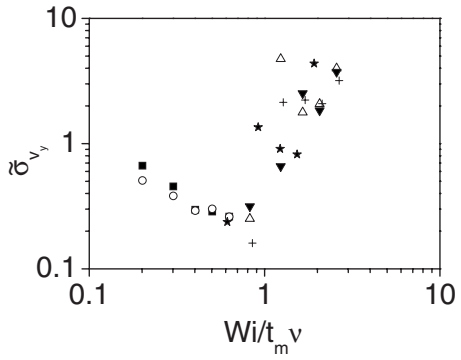


FIG. 20. 100:60 CPyCl-NaSal solution: space- and time-averaged rms fluctuations of the $y$ component of the velocity, as a function of the dimensionless control parameter $\chi \equiv \mathrm{Wi}/t_m\nu$, at the different driving frequencies (in Hz) 2.0 (■), 3.5 (○), 6.5 (⋆), 8.2 (△), 10.5 (▼), and 11.5 (+).

riod. Figure 19 shows the latter result, $\tilde{\sigma}_{v_y}(x)$, for different driving amplitudes.

At the lowest driving amplitude, 0.8 mm [Fig. 19(a)], for which the flow is always laminar, $\tilde{\sigma}_{v_y}(x)$ is nearly structureless and has a small magnitude at all driving frequencies. Fluctuations are slightly larger for the weakest forcing, simply because of the experimental uncertainty in the velocity measurements. At 1.2 mm [Fig. 19(b)] $\tilde{\sigma}_{v_y}(x)$ is still very small for the two lowest frequencies (laminar flow); for the second and third resonance frequencies it has a similar value as for 0.8 mm; for the second and third minima of the dynamic response, instead, it becomes large and peaked at the tube axis. Finally, at 1.6 mm [Fig. 19(c)] $\tilde{\sigma}_{v_y}(x)$ exhibits similar trends as at the previous driving amplitude for the three highest driving frequencies.

The time-averaged rms fluctuations of the velocity can also be integrated in space, to obtain a global magnitude $\tilde{\sigma}_{v_y}$, which behaves as an "order parameter" for the instability. The corresponding control parameter should be the Weissenberg number, given the elastic nature of the instability. However, since we are driving the flow at periods much shorter than $t_m$ (the relaxation time of the fluid) the driving period $(1/\nu)$ is possibly a more relevant time scale for the formation of the vortices than $t_m$. Considering this, we define a dimensionless control parameter

$$\chi \equiv \frac{\mathrm{Wi}}{t_m\nu} = \frac{2\pi z_0}{r_q}. \tag{6}$$

Figure 20 shows the behavior of $\tilde{\sigma}_{v_y}$ as a function of $\chi$ at the different driving frequencies. The onset of a secondary flow on top of the basic parallel shear flow is made manifest by a noticeable increase in this magnitude as vortices develop. Interestingly, the onset of the instability occurs at a value $\chi \simeq 1$.

### D. Birefringence measurements

We performed simultaneous PIV and qualitative birefringence measurements in our system, at forcing frequencies of 8.2 and 11.5 Hz and a forcing amplitude $z_0 = 1.2$ mm. Figure 21 shows the time evolution of the stress map at $\nu = 8.2$ Hz and $z_0 = 1.2$ mm. The time phase of each image corresponds approximately to the time phases of the velocity and vorticity maps in Fig. 10.

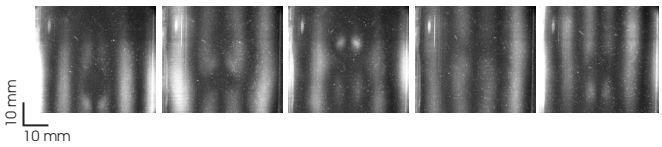


FIG. 21. Birefringence map for $\nu = 8.2$ Hz and $z_0 = 1.2$ mm. Time phases: 0, $T/4$, $T/2$, $3T/4$, and $T$.

Near the tube walls the stresses align vertically and are rather large at all time phases. On the contrary, in the central part of the flow the stress field depends strongly on the time phase. Stresses are distributed rather inhomogeneously in the vertical direction. Birefringent bands are wider at the center of the vortices at time phases $T/4$ and $3T/4$, when the vorticity is large. At time phases 0, $T/2$, and $T$, when the vorticity is small, the stress field relaxes and the bands break into small birefringent zones.

## IV. SUMMARY AND CONCLUSIONS

The periodic flow of a Newtonian fluid in a vertical pipe, driven by an oscillatory pressure gradient, is stable in the whole range of driving frequencies and amplitudes explored in the present experiments [17]. Our experiments with silicone oil show indeed that a relatively simple parallel shear flow is established, in which all the fluid moves in the same direction following the periodicity of the driving.

The behavior of the wormlike micellar solution CPyCl-NaSal 100:60 mM is rather similar at low driving frequencies. At higher driving frequencies, however, the laminar base flow turns out to be unstable at increasing driving amplitudes.

The structure of the laminar base flow is important to the development of the first instability. At the lowest driving amplitudes that make the flow unstable, two symmetric vortices (actually a cut of a single toroidal vortex) appear always where the shear rate is maximum in the laminar velocity profiles, in radial positions for which the velocity is relatively low. Indeed, vortices are present only at driving frequencies for which the laminar velocity profiles display alternating regions of upward and downward motion. This points to the large shear rates experienced by the fluid, at the quiescent points of the flow, as responsible for the first instability of the laminar base flow.

Since the driving amplitude $z_0$ in our experimental setup cannot be modified in a continuous way, we cannot answer the question whether the instability observed presents hysteresis. This information is relevant to ascertain the critical or subcritical nature of this first bifurcation. A modification of the setup that will allow us to modify $z_0$ (and thus the control parameter $\chi$) in a continuous way is currently in progress.

Elastic instabilities at very low Reynolds number have been reported only for flows with curved streamlines. In these flows the curvature of the streamlines gives rise to

elastic normal stresses that destabilize the flow, ultimately leading to elastic turbulence (or turbulence without inertia) [9,19,20]. Since shear flows of viscoelastic fluids with parallel streamlines do not give rise to normal stresses, it was the common thought that this kind of flow would not undergo elastic instabilities. However, Morozov and van Saarloos showed theoretically that parallel shear flows of purely viscoelastic fluids might be nonlinearly unstable [10]. Connecting with these predictions, we have presented an experimental scenario that allows the generation of parallel shear flows with large shear rates (high Wi) at small Re. This is achieved by the oscillatory driving, which makes the elastic properties of the fluid very important even in the laminar regime. It is important, however, to stress the fact that the micellar solution used in the present experiments presents shear thinning at high shear rates ($\dot{\gamma} > 0.1\ s^{-1}$) [13]. Since these shear rates are reached in most of our measurements, we cannot rule out that shear thinning plays a role in making the base flow unstable. The instability in this case would not be purely viscoelastic. We believe, however, that the essential ingredient to render the laminar flow unstable is its complex structure of alternating, stationary regions of upward and downward motion, which is entirely due to the elasticity of the fluid. More experimental work using complex fluids of different rheological behavior is needed to elucidate this point.

In conclusion, we have carried out PIV measurements of an oscillatory flow in a tube for a Newtonian and a Maxwell fluid with similar material properties. The oscillatory flow of the Newtonian fluid is stable in the whole range of parameters explored. The oscillatory flow of the Maxwell fluid is unstable at high driving frequencies, even though Re remains very small. The first instability observed gives rise to a toroidal vortex with axial symmetry and stationary. At increasing driving amplitudes these simple vortices are unstable and more complex structures are found. These results are potentially relevant in the search for experimental observations of a subcritical instability in parallel viscoelastic shear flows.

## ACKNOWLEDGMENTS

We are grateful to A. Morozov (Universiteit Leiden) for pointing out to us the interest in looking for instabilities in the oscillatory flow of complex fluids, and to him and W. van Saarloos (Universiteit Leiden) for interesting discussions. This research has received financial support through Projects No. FIS2006-03525 (MEC, Spain), No. SGR-2005-00507 (DURSI, Generalitat de Catalunya), and No. CONACyT 38538 (Mexico). A.A.C.P. acknowledges the support given by the Dorothy Hodgkin Foundation.

[1] J. A. del Río, M. López de Haro, and S. Whitaker, Phys. Rev. E **58**, 6323 (1998); **64**, 039901(E) (2001).
[2] D. Tsiklauri and I. Beresnev, Phys. Rev. E **63**, 046304 (2001).
[3] J. R. Castrejón-Pita, J. A. del Río, A. A. Castrejón-Pita, and G. Huelsz, Phys. Rev. E **68**, 046301 (2003).
[4] M. Torralba, J. R. Castrejón-Pita, A. A. Castrejón-Pita, G. Huelsz, J. A. del Río, and J. Ortín, Phys. Rev. E **72**, 016308 (2005).
[5] T. Drake and I. Beresnev, Am. Oil Gas Reporter, September issue, 101 (1999).
[6] E. Corvera-Poiré, J. A. del Río, and M. López de Haro, U.S. Patent No. 20050028971 (1994).
[7] A. A. Lambert, G. Ibáñez, S. Cuevas, and J. A. del Río, Phys. Rev. E **70**, 056302 (2004).
[8] A. C. T. Aarts and G. J. Ooms, J. Eng. Math. **34**, 435 (1998).
[9] P. Pakdel and G. H. McKinley, Phys. Rev. Lett. **77**, 2459 (1996).
[10] A. N. Morozov and W. van Saarloos, Phys. Rev. Lett. **95**, 024501 (2005).
[11] H. Rehage and R. H. Hoffman, J. Phys. Chem. **92**, 4712 (1988).
[12] J. F. Berret, J. Apell, and G. Porte, Langmuir **9**, 2851 (1993).
[13] A. F. Méndez-Sánchez, M. R. López-González, V. H. Rolón-Garrido, J. Pérez-González, and L. de Vargas, Rheol. Acta **42**, 56 (2003).
[14] R. J. Adrian, Annu. Rev. Fluid Mech. **23**, 261 (1991).
[15] E. Fischer and P. T. Callaghan, Europhys. Lett. **50**, 803 (2000).
[16] N. Z. Handzy and A. Belmonte, Phys. Rev. Lett. **92**, 124501 (2004).
[17] M. Hino, M. Sawamoto, and S. Takasu, J. Fluid Mech. **75**, 193 (1976).
[18] K. Arora, R. Sureshkumar, and B. Khomami, J. Non-Newtonian Fluid Mech. **108**, 209 (2002).
[19] A. Groisman and V. Steinberg, Nature **405**, 53 (2000).
[20] A. Groisman and V. Steinberg, Phys. Rev. Lett. **78**, 1460 (1997).